arXiv:cond-mat/0504728v1 [cond-mat.mtrl-sci] 27 Apr 2005

The nature of iron-oxygen vacancy defect centers in $PbTiO_3$

H. Meštrić, R.-A. Eichel,* T. Kloss, K.-P. Dinse, So. Laubach, St. Laubach, and P.C. Schmidt
Eduard-Zintl-Institute, Darmstadt University of Technology, D-64287 Darmstadt, Germany

K.A. Schönau, M. Knapp, and H. Ehrenberg
Materials Science, Darmstadt University of Technology, D-64287 Darmstadt, Germany

(Dated: 22 February 2005)

The Fe^{3+} center in ferroelectric $PbTiO_3$ together with an oxygen vacancy forms a charged defect associate, oriented along the crystallographic *c*-axis. Its microscopic structure has been analyzed in detail comparing results from a semi-empirical *Newman superposition model* analysis based on finestructure data and from calculations using density functional theory.

Both methods give evidence for a substitution of Fe^{3+} for Ti^{4+} as an acceptor center. The position of the iron ion in the ferroelectric phase is found to be similar to the B-site in the paraelectric phase. Partial charge compensation is locally provided by a directly coordinated oxygen vacancy.

Using high-resolution synchrotron powder diffraction, it was verified that lead titanate remains tetragonal down to 12 K, exhibiting a c/a-ratio of 1.0721.

Keywords: lead titanate ceramics, ferroelectrics, iron functional center, oxygen vacancy, charge compensation, EPR, Newman superposition model, DFT calculations

I. INTRODUCTION

Piezoelectric lead titanate oxide ($PbTiO_3$, PT) is of considerable scientific and technical interest because of its extraordinary electromechanical properties leading to the development of novel devices, such as nonvolatile memories, detectors, sensors or actuators[1,2,3]. A variety of ferroelectric properties can be controlled by replacing the lead or titanium cations with rare-earth or transition-metal ions. In general, the effect of aliovalent dopants on $PbTiO_3$, such as Fe^{3+}, leads to the creation of oxygen vacancies ($V_O^{\bullet\bullet}$) (The Kröger and Vink notation is used to designate the charge state of the defect with respect to the neutral lattice.) for charge compensation, which are expected to have a major impact on properties and performance of ferroelectric compounds. However, it is still not certain at which coordination sphere the charge compensation takes place, and because the oxygen vacancies are known to be the dominant charge carriers in this class of compounds this is an issue of technological and scientific importance[4]. Beside charge compensation provided by $V_O^{\bullet\bullet}$, intrinsic doubly negatively charged V''_{Pb} centers have been proposed as additional charge compensating mechanism[5], these vacancies, however, being rather immobile and almost of no importance for charge transport.

When dealing with dopants on a sub-percentage level, a sensitive test of the local environment around the functional center can only be provided by electron paramagnetic resonance (EPR). In case of paramagnetic Fe^{3+} dopants, the sextet spin ground state is most influenced by the ligand-field originating from the nearest-neighbor O^{2-} ions. The resulting finestructure (FS) interaction is a measure of the local symmetry. Various structure models have been proposed such as $Fe'_{Ti} - V_O^{\bullet\bullet}$ defect associates, not-coordinated 'free' Fe'_{Ti} centers, as well as off-center shifted iron centers. Previous EPR studies on crystalline samples reported FS parameters spanning a large range[6]. Structural information about the dopant site in $PbTiO_3$ and related compounds can be based on modelling the magnitude of the FS parameter, and therefore its accurate determination is an important issue. Because most samples are provided in polycrystalline form, it was important to demonstrate that FS parameters can reliably be determined even for polycrystalline compounds by invoking high-frequency-EPR[7].

Structure modelling can be performed using different levels of sophistication. For instance, the FS parameter can be analyzed in terms of the semi-empirical *Newman superposition model* (*NSM*)[8]. Within this model, values for local distortion, i.e., atomic displacements from the ideal crystal structure in the vicinity of the Fe^{3+} center, are derived by comparing calculated and observed FS parameters. A detailed study was performed already 25 years ago by Siegel and Müller[9,10], in which the distortion of the cubic high-temperature unit cell in the ferroelectric phase was taken as decisive parameter controlling the FS splitting at the iron site. Over the past decades, the *NSM* parametrization has been refined by applying the method to many examples of paramagnetic centers in perovskite-type crystals. Examples include iron-doped $PbTiO_3$, $SrTiO_3$ and $BaTiO_3$[9,10], $LiTaO_3$[11], as well as chromium-modified $PbTiO_3$[12] and manganese in $BaTiO_3$[13].

Second, an alternate approach offering additional microscopic information, is provided by calculating the equilibrium structure using density-functional theory (*DFT*). In recent years numerous calculations have been performed on ferroelectric materials in order to explain the microscopic mechanisms of spontaneous polarization[14,15] and phase diagrams[16,17], or to determine the full piezoelectric stress tensor and dynamical charges[20]. In particular, the role of defects and defect dipoles has been highlighted. Oxygen vacancies were shown to pin at 180°-domain walls, confirming the tendency of these defects to migrate to the walls[21]. It was

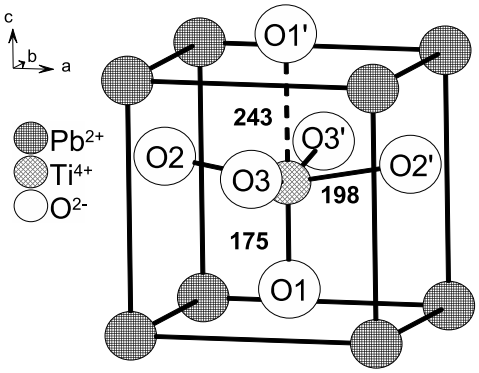


Figure 1: Schematic representation of the tetragonal unit cell of $PbTiO_3$ with designation of the different oxygen sites. The experimental atomic distances for the Ti-site to the surrounding oxygen octaeder are given in pm.

also derived that lead vacancies have stable charges ranging from -2 to -4 and thus being an effective acceptor in lead titanate[22]. The dipole moment $V_{\mathrm{O}}^{\bullet\bullet} - V_{\mathrm{Pb}}''$ of di-vacancies was calculated, demonstrating that the increased value may be an important source of local polarization and electric fields[23]. Another defect dipole originates from interstitial hydrogen impurities in lead titanate, which were found to bind to oxygen and to act as shallow donor impurities. The H-O dipole increases the polarization and the barrier for reversing the defect dipole, which can give rise to imprint[24].

In this work, we exploit the recently accurately determined FS parameter[7] as basis for structure modelling by performing an *NSM* analysis. Second, we compare the results obtained from this semi-empirical approach with results from *DFT* calculations, thus providing a sound basis for the postulated structural relaxation at the impurity site. As a result, we present a refined structural model of the iron functional center in lead titanate.

II. THEORETICAL METHODS

A. Newman superposition model

With its five unpaired electrons, the free Fe^{3+} ion possesses a half-filled $3d$ shell and can be described as orbital singlet. Its ground state configuration is ${}^6S_{5/2}$ ($S = \frac{5}{2}$) and the six-fold spin degeneracy can be lifted by the FS interaction and an external magnetic field. Neglecting hyperfine interaction, because the magnetic active isotope ^{57}Fe is present in only 2.2 % natural abundance, an approximate spin-Hamiltonian for this high-spin system can be written as

$$\mathcal{H} = \beta_e \mathbf{B_0} \cdot \mathbf{g} \cdot \mathbf{S} + \sum_{k,q} B_k^q O_k^q(S_x, S_y, S_z) \qquad (1)$$

Here, β_e denotes the Bohr magneton, $\mathbf{B_0}$ is the external magnetic field, $\mathbf{g}$ the electron $\mathbf{g}$-matrix, B_k^q are the FS Hamiltonian coefficients and O_k^q are the extended Stevens spin operators[25,26]. The first term represents the electronic Zeeman interaction and the second term is the effective FS Hamiltonian, describing the interaction of the crystal field with the paramagnetic ion. The rank k in the Hamiltonian must be even, and k is restricted by $k \leq 2S$ and $q \leq k$, allowing terms up to $k = 4$ for $S = \frac{5}{2}$. However, parameters b_k^q only up to second rank ($k = 2$) will be used, because terms of fourth rank were shown to be at least two orders of magnitude smaller than those of second rank[6](c-e). Parameters b_k^q are related to the standard FS parameters B_k^q by means of the scaling factor as $B_k^q = f_k b_k^q$. For $k = 2$ one finds $f_2 = \frac{1}{3}$. The coefficients b_k^q are related to the conventional spectroscopic FS parameters D and E by $b_2^0 = 3B_2^0 = D$ and $b_2^2 = 3B_2^2 = 3E$.

The FS term in (1) lifts the degeneracy of eigen states even in the absence of an external magnetic field. There is always a choice of spin-operator coordinate system with respect to the crystal axes for which the ratio b_2^2/b_2^0 lies in the interval $[0, 1]$, analogous to the condition $E/D \leq 1/3$.

In case the symmetry of the paramagnetic site is axial, the FS coefficients in its eigen frame reduce to $b_2^0 \neq 0$, $b_2^2 = 0$. Furthermore, the $\mathbf{g}$-matrix for S-state ions usually has very small anisotropy and can be treated as isotropic. The resulting scalar g value is expected to be close to that of the free electron g_e. For Fe^{3+} we therefore set $g_{\mathrm{iso}} = 2.002$ and then the spin-Hamiltonian used for numerical spectrum simulation of the experimental data reduces to

$$\mathcal{H} = \beta_e g_{\mathrm{iso}}\, \mathbf{B_0} \cdot \mathbf{S} + b_2^0 \left[S_z^2 - \frac{1}{3} S(S+1) \right] \qquad (2)$$

The *Newman superposition model*[8] allows for an analysis of positions of neighboring ions (ligands) around the Fe^{3+} center, given the single-ligand contributions $\bar{b}_k(R_i)$ are known. The essential assumption of the *NSM* is that the spin-Hamiltonian parameters for a paramagnetic ion can be constructed by a superposition from individual contributions of separate neighboring ligands. The contribution of next nearest neighbor ions as well as interaction between the ligands are ignored. The *NSM* expression for the zero-field splitting parameters can be formulated as follows

$$b_k^q = \sum_i \bar{b}_k(R_i)\; K_k^q(\theta_i, \phi_i) \qquad (3)$$

Here, i denotes every ligand, $\bar{b}_k$ is the contribution from each single ligand, R_i is the distance between the

ith ligand and the paramagnetic ion, θ_i and ϕ_i are the polar and axial angles between R_i and the symmetry axis of the paramagnetic center, and $K_k^q(\theta_i, \phi_i)$ are spherical harmonic functions of rank k of the polar angles, listed in[8](f). For the axial second-rank parameter one has

$$K_2^0 = \frac{1}{2}(3\cos^2\theta - 1) \tag{4}$$

For the short-range distance dependence of the single-ligand contribution, the following empirical power law was established

$$\bar{b}_k(R_i) = \bar{b}_k(R_0)\left(\frac{R_0}{R_i}\right)^{t_k} \tag{5}$$

The critical exponent parameter t_k is specific to a particular ion-ligand system. For a given ligand, the *intrinsic parameters* $\bar{b}_k(R_i)$ are determined by the nature of the ligand and the covalency of the bond, which is assumed to depend exclusively on the bond lengths R_i. Because $\bar{b}_k(R_i)$ in this model depends only on the ligand and its distance, and not on other properties of the host crystal, this parameter can be obtained from data of the same ion - ligand complex measured in other host crystals.

If the molecular coordinate system coincides with the principal axes system of the FS tensor, all off-diagonal elements vanish. For the Fe^{3+} ion at a position of tetragonal site symmetry ($4mm$), the *NSM* can be used in its truncated form[9]

$$b_2^0 = \bar{b}_2(R_0)\frac{3}{2}\sum_i \left(\frac{R_0}{R_i}\right)^{t_2}\left(\cos^2\theta_i - \frac{1}{3}\right) \tag{6}$$

The strategy followed is to calculate the FS parameter by using the *NSM* for different conceivable structural arrangements, and to compare the calculated values with the experimental data. The experimental value for b_2^0 has been determined reliably[7], and thus the interception points between the calculated curve and the experimental value is used for a prediction of actually realized local structure. Previously, the extremum of the calculated b_2^0 dependence was used to obtain an approximate ion position, although a correlation between the ZFS extremum and the ion equilibrium position cannot be derived from first principles.[9,10].

B. Density functional theory (*DFT*) modelling

The electronic structure of Fe:$PbTiO_3$ was calculated using two different *DFT* methods. First, the local relaxation of the structure around the defects, Fe_{Ti}, and V_O, is studied by the Vienna Ab initio Simulation Package (VASP)[27], as applied recently to study Pb-O vacancies in $PbTiO_3$[23]. However, instead of using ultrasoft pseudopotentials, Projector Augmented Waves (PAW) have been applied[28,29]. The identical basis set has been used, namely Pb($5d$,$6s$,$6p$), Ti($3s$,$3p$,$3d$,$4s$,$4p$), and O($2s$,$2p$), as well as the LDA exchange potential[30], and a $4\times4\times4$ k-mesh. Second, the electron density distribution $\rho(r)$ has been computed by the NFP (new full potential) program package[31,32,33], which is a variant of the LMTO (linear muffin-tin orbitals)[34] procedure using a minimal basis set.

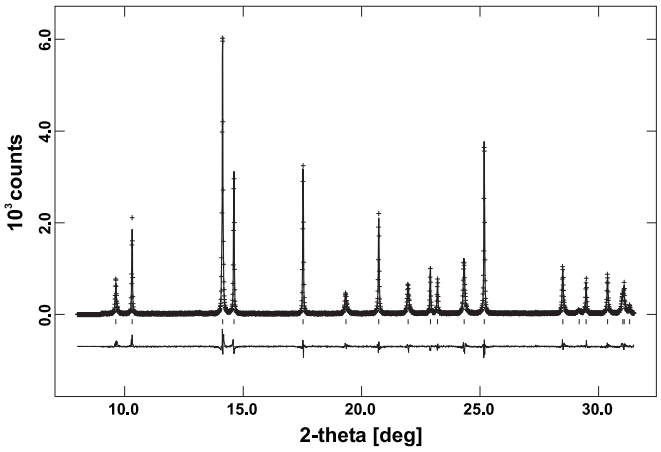


Figure 2: Observed and calculated diffraction profiles for $PbTiO_3$, obtained from high-resolution synchrotron powder diffraction at 12 K (top) together with their difference curve (bottom); $\lambda = 0.0699988$ nm.

III. RESULTS

A. Low-temperature X-ray data

The low temperature crystal structure of lead titanate has been the subject of some controversy over the past 50 years. Several X-ray and optical studies as well as dielectric measurements of PT samples indicated small anomalies in the temperature regions around 173 K and 123 K. These anomalies were detected as changes in the negative volume expansion coefficient in combination with superlattice reflections in powder samples[36] below 173 K and as changes in lattice parameters and birefringence in single crystals around 183 K. They were interpreted as a possible second order phase transition to a different tetragonal, later corrected into an antiferroelectric orthorhombic phase[37]. Moreover, this earlier claimed low-temperature tetragonal phase was assumed to transform into a further tetragonal phase around 113 K[38], which does not fit into the picture of having an orthorhombic phase present at this temperature range. However, neither in neutron powder profiles[39], nor in X-ray dilatometric and optical measurements using PT single crystals, additional evidence was seen for a structural transition at low temperatures[40]. First-principle studies[41] show that

Table I: Lattice parameters ($a, b = 389.0673(11)$ pm, $c = 416.7553(30)$ pm), cell volume (0.0630856(5) nm^3) and relative atom coordinates (upper rows) for $PbTiO_3$ at 12 K, obtained from high-resolution synchrotron powder diffraction. U_i is the mean square of atomic displacement. Also listed are the predicted values from *DFT* calculations with lattice parameters $a = b = 386.4$ pm, $c = 404.2$ pm (lower rows). Pb was kept fixed at the origin for both, Rietveld refinement and *DFT* calculations.

atom		X	Y	Z	$U_i \cdot 100$	site symmetry
Pb	exp.	0.000000	0.000000	0.000000	0.820(27)	4MM(001)
	DFT	0.000000	0.000000	0.000000		
Ti	exp.	0.500000	0.500000	0.5415(14)	0.66(10)	4MM(001)
	DFT	0.500000	0.500000	0.5346		
O1	exp.	0.500000	0.500000	0.1239(19)	0.38(19)	4MM(001)
	DFT	0.500000	0.500000	0.0904		
O2 / O3	exp.	0.000000	0.500000	0.6288(13)	0.38(19)	MM2(001)
	DFT	0.000000	0.500000	0.6032		

the thermodynamically stable phase at low temperatures is the tetragonal one, as all the unit-cell preserving distortions at low temperature have positive elastic constants and as there are no other mechanical instabilities present that could cause a transition to a lower symmetry group.

To identify the low-temperature structure and to obtain reference values for the interpretation of EPR data recorded at low temperatures, a high-resolution synchrotron powder diffraction experiment was carried out in reflection geometry at B2, Hasylab in Hamburg, Germany (figure 2). The measurement was performed at 12 K using a He closed-cycle cryostat, equilibrating the temperature in a low-pressure helium atmosphere. The powdered sample was glued onto a Si (711) low-background wafer and measured using an incident beam of wavelength 0.0699988 nm in combination with an analyzing crystal and a scintillation counter[42].

For Rietveld refinement, the general structure analysis system (GSAS)[43] was used. As the peak profiles of the ferroelectric material are quite complex, the profiles were fitted using the incorporated generalized model for anisotropic peak broadening[44]. The structural model could be refined with the symmetry of $P4mm$, keeping the lead positions fixed at the origin. No superlattice reflections were detected. The c/a - ratio is 1.0721 at this temperature. Lattice parameters and atom coordinates obtained are given in table II B.

The detected low-temperature $P4mm$ symmetry is consistent with the interpretation of the EPR spectra, for which a FS tensor of axial symmetry was used, thus indicating that no orthorhombic phase is present[7]. Therefore it can be concluded that $PbTiO_3$ remains tetragonal down to 12 K, as already assumed earlier[41].

B. Superposition-model analysis

The intrinsic *NSM* parameters t_2 and $\bar{b}_2(R_0)$ have not yet been determined for iron centers in lead titanate. However, they may be adopted from similar single crystals having equivalent $Fe^{3+}-O^{2-}$ bonds in octahedral coordination. For Fe^{3+} in MgO at the central site with octahedral oxygen coordination, the following set of *NSM* parameters was reported: $\bar{b}_2 = -12.3514$ GHz, $t_2 = 8$, $R_0 = 210.1$ pm[9]. The ionic positions of the nearest oxygens were taken from the X-ray data at 12 K (cf. section III A). Because the site symmetry defines the direction of FS-tensor axes, the principal FS axis of the Fe^{3+} center was chosen along [0 0 1].

The common reference structure for undistorted cubic $PbTiO_3$ is the perovskite structure, in which Ti^{4+} ions are octahedrally coordinated by oxygen ions and are positioned at the center of the unit cell. The Pb^{2+} ions are twelvefold coordinated by oxygens and are located at the corners of the cube, whereas the O^{2-} ions are centered on each face of the unit cell. In the ferroelectric tetragonal phase, the oxygen octahedron is elongated along [0 0 1] and also shifted by 54 pm with respect to the Pb^{2+} position, the titanium ion being displaced from the center of cell along [0 0 1] by 17 pm, respectively. As a result, the titanium ion occupies an *off-center* position within the shifted oxygen octahedron (cf. table II B, figures 1, 4).

Iron is believed to substitute Ti^{4+} as Fe^{3+} at the B-site in the ABO_3 perovskite structure. In order to ver-

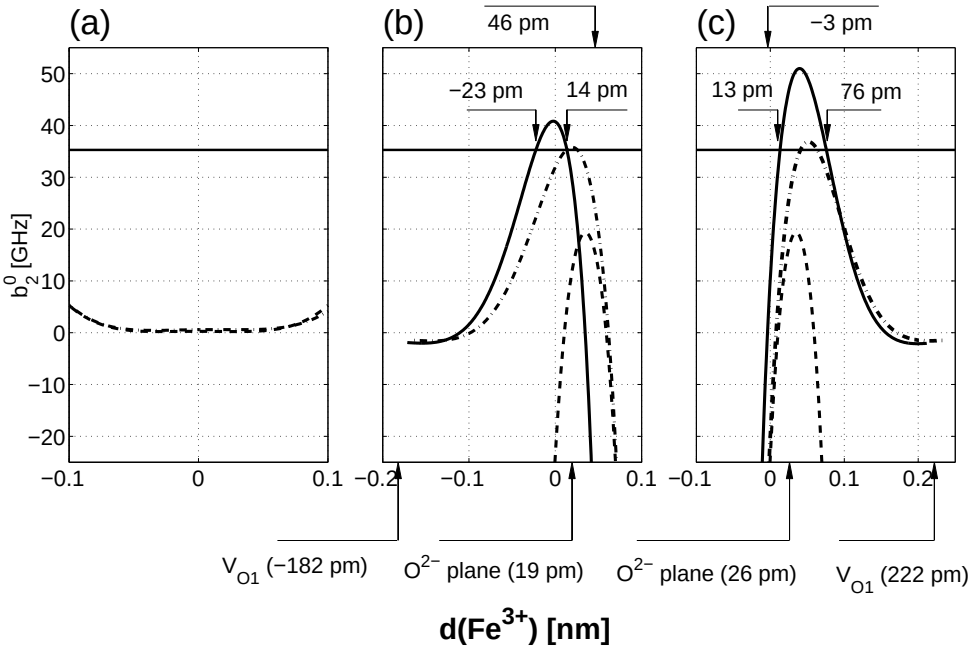


Figure 3: Comparison of the experimentally obtained axial FS parameter $b_2^0 = 35.28$ GHz (solid horizontal line) for the Fe^{3+} center in $PbTiO_3$[7] with calculated values for b_2^0 obtained from the *NSM* analysis in dependance of the displacement d from the Ti^{4+} position. The positions of the oxygen vacancies, of the center of the oxygen octahedra, as well as of the DFT-calculated shifts of the Fe^{3+} ion are indexed by arrows as reference. (a) - substitution of the Fe^{3+} ion either at the A-site. (b,c) - substitution of the Fe^{3+} ion at the B-site with oxygen vacancies either at O1 or O1'. The model for 'free iron', i.e. without an oxygen vacancy in the nearest neighbor shell, is represented in all models by a dashed line and the model for the iron-oxygen vacancy associate by a dash-dotted line in case of static oxygen position and by a solid line for the model using relaxed oxygen positions.

ify this hypothesis, in the calculation we also considered the possibility that it substitutes at the A-site for Pb^{2+}. Furthermore, to decide whether the oxygen vacancy is situated in the first coordination sphere or if it is located more distantly, two more structure models were investigated, with and without oxygen vacancy in nearest neighbor positions. The model of a directly coordinated oxygen vacancy can be realized in two different arrangements, in which the vacancy may substitute either for the apical O1 or O1' position (cf. figure 1). A vacancy coordination at the equatorial O2 and O3 positions can be excluded as the orientation of the $Fe'_{Ti} - V_O^{\bullet\bullet}$ defect dipole has to be along the c-axis, due to the EPR results that indicate axial symmetry at the iron center[7]. For orientations of the oxygen vacancy along the a and b axes, the FS tensor would be of only orthorhombic symmetry. For a final model, the effect of a likely relaxation of oxygen ion positions in case of a directly coordinated oxygen vacancy has been taken into account. The relaxed ionic positions were obtained from the *DFT* calculations (cf. section III C).

The position of the oxygen octaeder is defined using the crystal coordinate system given in table II B. Here, the oxygen vacancy is located either at (0.5000 0.5000 0.1239), or at (0.5000 0.5000 1.1239) in fractional coordinates, and the reference position of iron is at the titanium position in the undoped system at (0.5000 0.5000 0.5415). For the calculation of b_2^0, the position of Fe^{3+} was varied along [0 0 1], the parameter d defining the shift of the ion. A positive sign of d defines a shift towards the O1' oxygen, i.e. $d = z \times 416.8$ pm.

The results are presented in figure 3, depicting the dependence of calculated axial FS parameters b_2^0 on d for the different structural models. In this figure, the experimentally obtained value for b_2^0 is represented by a solid horizontal line. As reference, the positions of the corresponding oxygen vacancies $V_{O1}^{\bullet\bullet}$, $V_{O1'}^{\bullet\bullet}$, the position of the equatorial plane of oxygens through O2, O3, as well as the positions for the iron as obtained by the DFT calculations (cf. section III C) are indicated by arrows.

Four conclusions immediately emerge from the NSM calculations: as compared to earlier studies for the iron center in lead titanate[9,10], in which static oxygen positions were used, the inclusion of relaxed positions for the equatorial oxygens towards the vacancy yields substantially refined and quite different curves for b_2^0. Furthermore, the extremum of the b_2^0 dependence is no a-priori viable position for the iron displacement as has earlier been exploited as first guess[9,10]; the intersection points with the experimental value, not necessarily coinciding with the extremum, should be used instead. Finally, agreement with the experimental value[7] can be obtained

only with a model, in which Fe^{3+} is substituted at the B-site with a directly coordinated oxygen vacancy, thus forming an $Fe'_{Ti} - V_O^{\bullet\bullet}$ defect associate.

In the pure, unsubstituted ferroelectric phase, Ti^{4+} is displaced considerably from the center of the oxygen octahedron (cf. table II B). In contrast, there are two predicted positions for the Fe_{Ti}^{3+} ion with an adjacent oxygen vacancy for each of the two models: for the $Fe'_{Ti} - V_{O1}^{\bullet\bullet}$ associate the iron ion is either displaced by 14 ± 5 pm from the Ti^{4+} position away from the vacancy towards the center of the truncated octahedron, or it is shifted considerably by 23 ± 5 pm towards the vacancy. For the alternative $Fe'_{Ti} - V_{O1'}^{\bullet\bullet}$ associate, the Fe_{Ti}^{3+} ion both times is shifted towards the vacancy, where one position is close to the plane of equatorial oxygens at 13 ± 5 pm and the other position is at 76 ± 5 pm. In order to distinguish between these positions, further information as provided by the *DFT* calculation is needed. The finally preferred structure (vide infra) of the $Fe'_{Ti} - V_O^{\bullet\bullet}$ defect associate from the *NSM* calculations is presented in figure 4.

C. *DFT* calculations

1. *DFT investigations of undoped $PbTiO_3$*

First, the iron-free host lattice of $PbTiO_3$ was studied. Using the VASP code, lattice parameters $a = 386.6$ pm and $c = 403.9$ pm were obtained, which is in agreement with earlier calculations[35]. These values are smaller than the experimental values as expected from LDA calculations. The percentage difference between the experimental and calculated values are different for the a and c direction resulting in a calculated c/a strain of 1.04 compared to the experimental value of 1.07. The calculated Ti-O bonds are given in figure 4(c).

Next, one oxygen vacancy was inserted in the $2 \times 2 \times 2$ supercell without providing charge compensation, i.e., the electronic structure of $Pb_8Ti_8O_{23}$ was calculated for a determination of the local relaxation of the ions around the vacancy. As shown in figure 4 (d), one finds that the nearest neighbor Ti ions move away from the vacancy site, which was also predicted in a previous LDA calculation[18]. If the vacancy is located at the O1 site (cf. figure 1), the Ti moves towards O1' and the Ti-O1' distance decreases in the LDA simulation from 224.5 pm (in the perfect lattice) to 193.2 pm. The Ti ion closest to the vacancy in positive c-direction moves from its original position by $d = +25.4$ pm while the nearest Ti ion on the opposite side of the vacancy is displaced by $d = -3.9$ pm. If the vacancy is located at the O2 site, Ti moves towards the O2' site and the Ti-O2' bond distance decreases from 195.3 pm to 187.6 pm.

2. *DFT investigations of iron-doped $PbTiO_3$*

The theoretical studies of the system Fe':$PbTiO_3$ have been performed using an $2 \times 2 \times 2$ supercell, in which now Ti is partly replaced by Fe. We have studied different possibilities of ion arrangements for the defect structures. In a model series A, we have replaced two Ti by Fe', Fe'_{Ti}, and for charge compensation we have created one O vacancy, $V_O^{\bullet\bullet}$, that is the supercell has the composition $Pb_8Ti_6Fe_2O_{23}$. In two other model series, we have replaced only one Ti by Fe'. In the model series B, we consider the neutral defect $[Pb_8Ti_7FeO_{23}]$ and in the model series C, the charged defect $[Pb_8Ti_7FeO_{23}]^+$, charge compensation obtained by assuming a homogeneously charged background.

The ion arrangement in the three model series A to C are as follows. In model A1, the two Fe'_{Ti} are next nearest neighbors and the $V_O^{\bullet\bullet}$ is located between these two Fe'_{Ti} forming a clustered defect oriented in the c direction. Model A2 differs from model A1 only by the assumption that one of the Fe'_{Ti} is an isolated point defect, whereas for model A3, we have assumed that all point defects are isolated. Model A4 to A6 vary from model A1 to A3 by the position of the oxygen vacancy, which is located in the a (or b) direction (i.e., at O2 or O3 in figure 1) rather than in the c direction (O1 in figure 1). For the systems of model series B $[Pb_8Ti_7FeO_{23}]$ and C $[Pb_8Ti_7FeO_{23}]^+$ with only one Fe_{Ti} in the $2 \times 2 \times 2$ supercell we have again studied the arrangement of $V_O^{\bullet\bullet} - Fe'_{Ti}$ neighbored in a or c direction (models B4 or B1, B2 and C4 or C1, C2) as well as the arrangement with both Fe'_{Ti} and $V_O^{\bullet\bullet}$ as isolated point defects (models B3 and C3). For the defect associate $V_O^{\bullet\bullet} - Fe'_{Ti}$ neighbored in the c direction we distinguished between the case where the vacancy site is at O1 (models B1 and C1) or at O1' (models B2 and C2) as the distances of the O1 and O1' to Fe'_{Ti} are not the same.

For all these models we have performed a structure optimization varying the atomic positions but taking the lattice constants a and c fixed to the values obtained from the DFT results for the pure host lattice given in table II B. Considering the total energy of the optimized structures it is concluded for all three model series A to C that the oxygen vacancy in c direction is always favored in energy, as compared to an orientation along a. For models A1 to A6 the clustered defect $Fe'_{Ti} - V_O^{\bullet\bullet} - Fe'_{Ti}$ along the c direction (model A1) gives the lowest energy E_{A1} followed by model A2 ($Fe'_{Ti} - V_O^{\bullet\bullet}$ placed along the c direction) with energy E_{A2}, where $E_{A2} - E_{A1} = 0.59$ eV per supercell.

Also for the model series with only one Fe'_{Ti} defect the direction of the $Fe'_{Ti} - V_O^{\bullet\bullet}$ associate along c (models B1 and C1) is preferred over the a direction. More precisely, the most stable arrangement is the arrangement were O1 is missing and not O1'. The models B1 and C1 are lower in energy than B2 and C2, namely $E_{B2} - E_{B1} = 0.35$ eV and $E_{C2} - E_{C1} = 0.34$ eV. The arrangements B4 and C4 with an orientation of the $Fe'_{Ti} - V_O^{\bullet\bullet}$ dipole along the

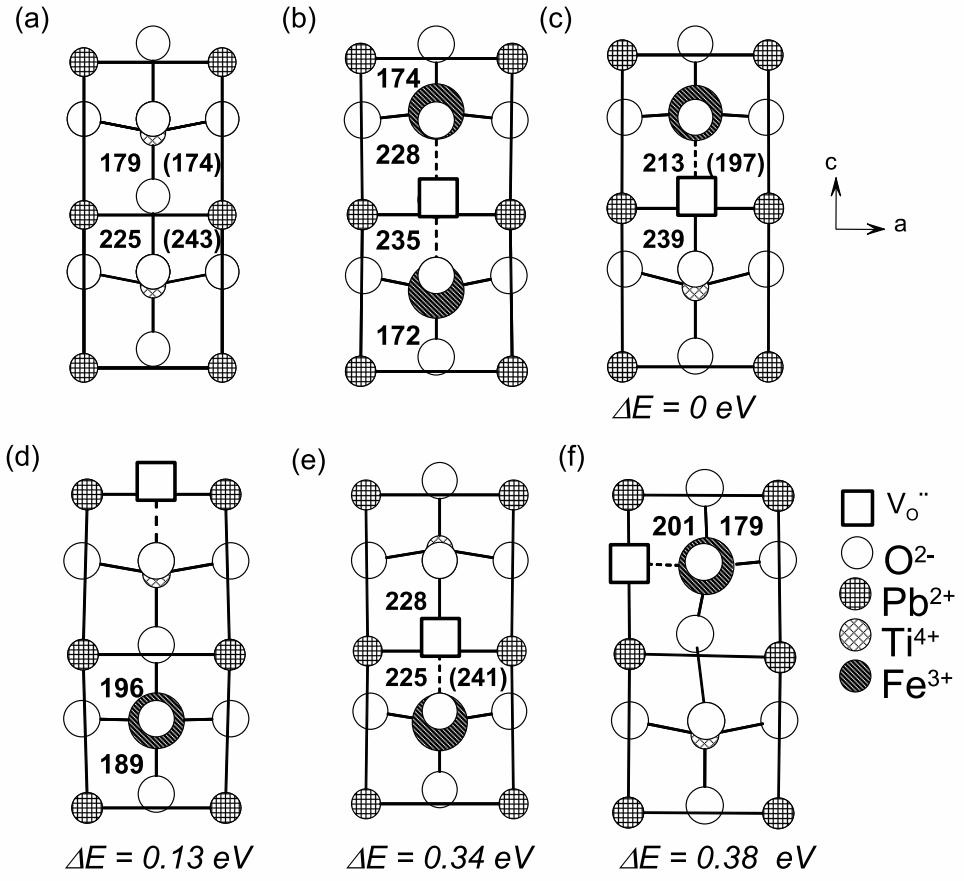


Figure 4: Comparison between the different structure models for Fe:$PbTiO_3$ deduced from the theoretical and experimental investigations. The given numbers indicate atomic distances (in pm) calculated by *DFT* (cf. section 3.3.2) and the bracketed values are experimentally and semi-emprically obtained values. The relative energies for comparable models are shown below the figures.
(a) undoped reference structure obtained from DFT calculations and from synchrotron powder difraction (cf. table II B);
(b) Fe'_{Ti}-$V_O^{\bullet\bullet}$- Fe'$_{Ti}$ complex in $Pb_8Ti_6Fe_2O_{23}$ oriented along *c*-axis (model A1);
(c) Fe'_{Ti}-$V_O^{\bullet\bullet}$ defect associate in $[Pb_8Ti_7FeO_{23}]^+$ oriented along *c*-axis where the O1 oxygen is missing (shorter bond, model C1). The bracketed values are obtained with Newman superposition model on the basis of measured FS data. This model is the energetically most favored among models with one oxygen vacancy.
(d) Fe'_{Ti} and $V_O^{\bullet\bullet}$ as isolated defects in $[Pb_8Ti_7FeO_{23}]^+$ (model C3);
(e) Fe'_{Ti}-$V_O^{\bullet\bullet}$ defect associate in $[Pb_8Ti_7FeO_{23}]^+$ oriented along *c*-axis where the oxygen O1′ is missing (longer bond, model C2);
(f) $Fe'_{Ti} - V_O^{\bullet\bullet}$ defect associate in $[Pb_8Ti_7Fe_2O_{23}]^+$ oriented along *a*-axis where the oxygen O2 is missing (model C4);
Models B1-B4 which consider defects in charged $Pb_8Ti_7Fe_2O_{23}$ are in the same energetical sequence.

a axis is less stable than the favored arrangement within the model series by $E_{B4}-E_{B1} = 0.45$ eV and $E_{C4}-E_{C1} = 0.38$ eV. The associated defect $Fe'_{Ti} - V_O^{\bullet\bullet}$ is favourable compared to the isolated defects by $E_{B3}-E_{B1} = 0.27$ eV and $E_{C3} - E_{C1} = 0.13$ eV. Applying the spin-polarised version of the LDA method changes the energy by less than 0.02 eV per $2 \times 2 \times 2$ supercell and therefore has not been pursued any further.

Next, the movement of the ions around the vacancy shall be described. Qualitatively, we find the same trends for all models considered here, namely the cation nearest to the vacancy moves away from the vacancy site, which results in a shortening of the metal oxygen bond opposite to the vacancy.

Comparing the undoped structure (figure 4 (a)) and the defect structures (figure 4 (b)-(f)) one sees that the position of the metal ion above the vacancy moves upwards above the plane of the four oxygen ions which has already been found for Ti_{Ti} in a previous calculation by Park and Chadi[18]. The displacement of the Fe ion from the original Ti position in the undoped host lattice represented by the distance *d* is equal to +46.6 pm and −11.6 pm for the two Fe'_{Ti} in model A1. For the structures with only one Fe'_{Ti} we get the following values for *d*,

$d_{A2} = +32.9$ pm $d_{B1} = +31.2$ pm, $d_{C1} = +33.5$ and $d_{C2} = -6.8$ pm.

Considering the atomic arrangement and relaxation we finally point out that even for the pure host the weak O - Ti bond of 243 pm compared to the other O - Ti bonds of 174 and 198 pm are not described quite satisfactorily by the LDA results, see figure 4. This also holds for GGA (Generalized Gradient Approximation) calculations which we have additionally performed using the potential of Perdew and Wang[45]. Therefore, we have repeated all calculations under the constrain of leaving the strain constant, $c/a = (c/a)_{exp} = 1.0721$ by both LDA and GGA. From these additional calculations we get the same main conclusions described above, namely that the associate $Fe'_{Ti} - V_O^{\bullet\bullet}$ in c direction has the lowest energy and compared to the original Ti and O positions the Fe'_{Ti} is moving away from the vacancy $V_O^{\bullet\bullet}$.

The resulting electron states are presented in figure 5, in which the density of states (DOS) and the partial DOS based on the Mulliken population analysis is plotted for $PbTiO_3$ (figure 5 (a)). The lowest states in figure 5 (a) are the $6s$-like states of Pb. Above these states we find the oxygen $2p$-like states mixing with the $6s$- and $6p$-like states of Pb and the $4s/4p$-like states of Ti. This indicates that the bonding has a distinct covalent character as found also in previous calculations[15,18,46]. The lowest states of the conduction bands are predominantly $3d$-like states of Ti for pure $PbTiO_3$. For $Pb_8Ti_6Fe_2O_{23}$ in figure 5 (b), additional $1s$ and $2p$ basis functions centered at the vacancy site have been used. No new states are found in the band gap, which otherwise would indicate the existence of color centers at the oxygen vacancy. Compared to figure 5 (a) we get additional Fe like states and one can see that the highest occupied states are now the $3d$-like states of Fe. The oxygen, for which the partial DOS are displayed in figure 5(b), is neighbored to Fe in the c-direction and labelled as O(Fe′). Its $2p_z$-like states show a common peak with the $3d$-like states of Fe in an energy range of -7 to -6 eV indicating an Fe - O bond.

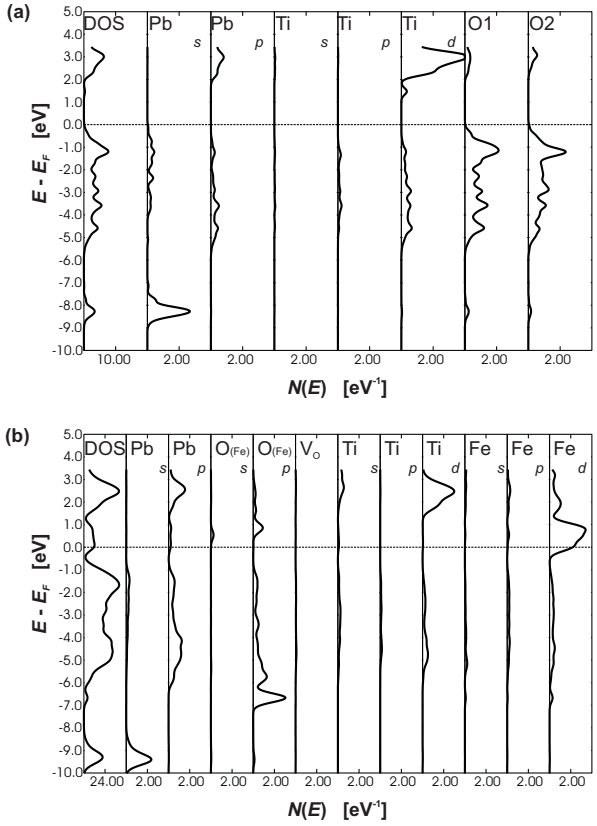


Figure 5: Density of states (DOS) for undoped $PbTiO_3$ (a) and Fe:$PbTiO_3$ (b). Total DOS and partial DOS of Pb, Ti(s, p, d), O1-3(s, p). The horizontal dotted line corresponds to the top of the valence band.

IV. DISCUSSION

The most striking prediction from the *NSM* calculations is that the Fe^{3+} functional center in lead titanate forms a charged $Fe'_{Ti} - V_O^{\bullet\bullet}$ defect associate with an oxygen vacancy in the local oxygen octahedron, the iron being substituted at the B-site of the perovskite ABO_3 lattice. The similarity of ionic radii between Ti^{4+} at 68 pm and Fe^{3+} at 64 pm as compared to Pb^{2+} with a radius of 124 pm supports this assignment. In fully or partly ionic compounds, vacancies are charge balanced by other defects forming an overall neutral system. It can be assumed that partial charge compensation takes place at a nearest-neighbor oxygen site in the octahedron, because the resulting Coulomb interaction is the most important driving force for association. This assignment is in accordance with first-principle calculations that predict the binding of oxygen vacancies to acceptor-type impurities[19], as well as to our *DFT* investigations that favor defect associates. Experimental findings indicate, however, that for other acceptor centers in similar compounds, like chromium-doped $PbTiO_3$[12] and copper-modified $Pb[Zr_{0.54}Ti_{0.46}]O_3$[48], no such association is present. Alternatively, like in iron-doped $SrTiO_3$, an equilibrium between 'free' Fe'_{Ti} centers and $Fe'_{Ti} - V_O^{\bullet\bullet}$ defect associates can be present[49]. With respect to the ionic mobility of free oxygen vacancies, the iron - oxygen vacancy defect dipole complex will be rather immobile in the ceramic. Hence, charge transport will be considerably hindered. Furthermore, the charged defect agglomerate may influence the poling properties by providing pinning centers for domain walls[50]. Moreover, dipolar defect complexes have been demonstrated to be able to also pin the polarization of the surrounding crystal[19]. In particular, oxygen-vacancy related defect dipoles have been shown to be involved in voltage offsets leading to imprint failure[51] and are suggested to play a crucial role in electrical fatigue[19,52,53].

With respect to the reliability of the predictions obtained by the semi-empirical *NSM* approach, the follow-

ing points should be mentioned. First, crystal distortions near the substituted ion and contributions from ions or vacancies more distant than neighboring ligands are neglected. Second, the main assumption of the *NSM* is that the spin-Hamiltonian parameters result from individual crystal field contributions of every nearest neighbor ion. Finally, the model is based upon the calculation of single electron-derived charge densities, whereas the FS interaction is related to two-electron expectation values. Apparently, the *NSM* has proven to yield reliable results for determining the second- and fourth-rank finestructure parameters in *S*-state ions, probably because the intrinsic parameters have been refined over several decades using a large set of experimental data. If iron at a B-site of the perovskite ABO_3 lattice can be considered as part of this set, the structural data can be considered as reliable.

Within these limits, the results can be interpreted as follows: the Fe^{3+} ion with the nearby oxygen vacancy probably has a position near the center of the truncated oxygen octahedron, i.e. at the (0.5000 0.5000 0.6288) position, whereas the second position in accordance with *NSM* prediction can be discarded because of *DFT*-based results.

As mentioned above, for all *DFT* calculations a $2\times2\times2$ unit cell was used. This size of the unit cell seems to be too small to avoid interaction of the defects, and the relaxation at the defect site could be smaller if larger unit cells are used. However, for computation time reasons we could not expand our unit cell. Nevertheless, it is most encouraging to find that the local structure with respect to Fe^{3+} positioning, predicted by *DFT* calculation and by the semi-empirical model are quite similar. The agreement is surprisingly good and might be fortuitous, considering the rather small supercell accomplished by an effective 12.5 % iron doping

The quantum mechanical simulations show, that the association of the defects is preferred over the arrangement as isolated point defects. Additionally, the arrangements for an orientation of the defect associate along the *c*-axis are more stable than the ones along the *a* and *b*-axes, confirming the conclusion drawn from the axial symmetry of the FS tensor[7]. The off-center position of the Fe ion in the oxygen octahedron leads to two $Fe'_{Ti} - V_O^{\bullet\bullet}$ distances in c direction and therefore to two different positions of the oxygen vacancy. According to the DFT investigations the vacancy at the O1 position in figure 1 is energetically favored, in which the long O1'-Fe'_{Ti} distance decreases significantly.

Finally, because the observed EPR spectra[7] can almost exclusively be interpreted in terms of $Fe'_{Ti} - V_O^{\bullet\bullet}$ associates, one can conclude that no 'free' Fe^{3+} signals, i.e., iron ions without associated $V_O^{\bullet\bullet}$ and hence with considerably smaller FS values, are present. Considering the condition for overall charge compensation there is a charge mismatch, because the Fe^{3+} ion substituting for the Ti^{4+} ions are singly negative charged (Fe'_{Ti}), whereas the associated oxygen vacancy is doubly positive charged ($V_O^{\bullet\bullet}$) with respect to the neutral lattice. Hence, additional mechanisms for charge compensation have to be discussed. Candidates for charge compensation are either free electrons (e') trapped in the lattice, lead vacancies (V''_{Pb}), and the formation of positively charged cations, such as $Pb^{2+} \rightarrow Pb^{+}$, $Ti^{4+} \rightarrow Ti^{3+}$, or $Fe^{3+} \rightarrow Fe^{2+}$. However, there no evidence for color centers in the *DFT* calculations and the variable valency ions Pb^{+}, Ti^{3+} are paramagnetic with g-values at about $g \approx 2.0$ to 1.9, which were not observed in the EPR spectra and thus can be excluded. Since intrinsic double negatively charged lead vacancies V''_{Pb} have been suggested as additional charge compensation[5], the overall electroneutrality condition for iron-modified lead titanate thus is proposed to be given by

$$[V_O^{\bullet\bullet}] = [Fe'_{Ti}] + \frac{1}{2}[V''_{Pb}] \tag{7}$$

This model is supported by the inherent loss of PbO during processing, for which reason a natural intrinsic $V_O^{\bullet\bullet} - V''_{Pb}$ di-vacancy pair was proposed[54], its existence, however, being currently controversially discussed on the basis of *DFT* calculations[22,23].

In principle, charge-compensation could also be obtained by the creation of $Fe'_{Ti} - V_O^{\bullet\bullet} - Fe'_{Ti}$ defect associates without the need for lead vacancies at all. The existence of such a defect structure is also supported by the *DFT* results, predicting this arrangement as of lowest energy. In this structure, the *DFT* calculations predicts two different iron sites, for which reason two Fe^{3+} EPR spectra with different FS parameters are expected. Using the calculated displacements of $d = +46.6$ pm and -11.6 pm, the corresponding *NSM* estimates are $b_2^0 = 9.6$ GHz and $b_2^0 = -34.7$ GHz, respectively. These values differ considerably from the experimentally obtained one, and for this reason this model can be discarded. Furthermore, for samples with low iron doping, this prediction of an $Fe'_{Ti} - V_O^{\bullet\bullet} - Fe'_{Ti}$ defect associate might not be upheld. Finally, from the present EPR experiment there is no further evidence for this hypothesis, because no indication for strongly dipolar coupled iron centers is detected in the EPR spectra.

V. CONCLUSION

In summary, a charged $Fe'_{Ti} - V_O^{\bullet\bullet}$ defect associate in lead titanate has been identified and its microscopic structure has been determined based on a comparison of FS data with results of semi-empirical *NSM* and *DFT* calculations. The refined structure comprises information about the structural relaxation around the iron functional center in lead titanate. In the model presented, Fe^{3+} is substituted as an acceptor center at the perovskite B-site with a directly coordinated oxygen vacancy. The position of the iron ion in the ferroelectric phase is found to be almost centered in the unit cell, different from the bulk B-site Ti^{4+} ions in the ferroelectric

phase that are considerably displaced, but similar to the B-site positions in the paraelectric phase.

The orientation of the $Fe'_{Ti} - V_O^{\bullet\bullet}$ defect dipole is found to be along the crystallographic c-axis. This can be concluded from EPR results which indicate axial symmetry at the iron center. Any other orientation of the defect dipole would result in an FS tensor of lower than axial symmetry. Furthermore, the *DFT* calculations confirm this assignment by showing that the total energy of the arrangement along the c-axis is more stable than the ones along the a and b-axes. Using high-resolution synchrotron powder diffraction, a quite large c/a-ratio of 1.0721 was measured, again pointing to the uniqueness of structural relaxation along c.

The impact of iron-doping in lead titanate on the macroscopic piezoelectric properties can now be rationalized from a microscopic point of view, because the iron - oxygen vacancy defect dipole complex will be rather immobile in the ceramic as compared to the ionic mobility of free oxygen vacancies. Thus, charge transport will be considerably hindered and the charged defect agglomerate may furthermore influence domain-wall motion and poling properties by providing pinning domain walls.

VI. ACKNOWLEDGMENTS

This investigation has been financially supported by the DFG priority program 1051 *'High-Field EPR in Biology, Chemistry and Physics'* and center of excellence 595 *'Electrical Fatigue in Functional Materials'*. The authors are grateful to helpful comments of the referees made during the review process. Furthermore, we thank Dr. D.J. Keeble for sending us a preprint about his X-band EPR study of Fe^{3+} centers in lead titanate single crystals prior to publication.

* corresponding author, fax: +49-6151-164347, e-mail: eichel@chemie.tu-darmstadt.de

[1] M.E. Lines, A.M. Glass: *Principles and applications of ferroelectrics and related materials*, Oxford University Press, Oxford (2001)
[2] W.L. Swartz, IEEE Trans. Electr. Insul. **25** (1990) 935-987
[3] J.F. Scott, Ferroelectrics Rev. **1** (1998) 1
[4] (a) D.M. Smyth, Annu. Rev. Mater. Sci. **15** (1985) 329; (b) *ibid.* Ferroelectrics **116** (1991) 117; (c) M.V. Raymond, D.M. Smyth, J. Phys. Chem. Solids **57** (1996) 1507
[5] (a) W.L. Warren, G.E. Pike, K. Vanheusden, D. Dimos, B.A. Tuttle, J. Robertson, J. Appl. Phys. **79** (1996) 9250-9257; (b) W.L. Warren, B.A. Tuttle, F.C. Rong, G.J. Gerardi, E.H. Poindexter, J. Am. Ceram. Soc. **80** (1997) 680-684
[6] (a) D.J.A. Gainon, Phys. Rev. **134** (1964) A1300-A1301; (b) G. Wessel, H. Goldick, J. Appl. Phys. **39** (1968) 4855; (c) R.G. Pontin, E.F. Slade, D.J.E. Ingra, J. Phys. C **2** (1969) 1146; (d) O. Lewis, G. Wessel, Phys. Rev. B **13** (1976) 2742-2746; (e) V.V. Laguta, M.D. Glinchuk, I.P. Bykov, Y.L. Maksimenko, J. Rosa, L. Jastrabik, Phys. Rev. B **54** (1996) 12353-12360
[7] H. Meštrić, R.-A. Eichel, K.-P. Dinse, A. Ozarowski, J. van Tol, L.C. Brunel, J. Appl. Phys. **96** (2004) 7440-7444
[8] (a) D.J. Newman, Adv. Phys. **20** (1971) 197; (b) D.J. Newman, W. Urban, J. Phys. C **5** (1972) 3101; (c) *ibid.*, Adv. Phys. **24** (1975) 793; (d) D.J. Newman, E. Siegel, J. Phys. C **9** (1976) 4285; (e) D.J. Newman, J. Phys. C **15** (1982) 6627-6630; (f) D.J. Newman, B. Ng, Rep. Prog. Phys. **52** (1989) 699-763
[9] E. Siegel, K.A. Müller, Phys. Rev. B **19** (1979) 109-120
[10] E. Siegel, K.A. Müller, Phys. Rev. B **20** (1979) 3587-3596
[11] T.H. Yeom, J. Phys. Condens. Matter **13** (2001) 10471-10476
[12] E. Erdem, R. Böttcher, H.C. Semmelhack, H.J. Gläsel, E. Hartmann, phys. stat. sol. (b) **239** (2003) R7-R9
[13] R. Böttcher, C. Klimm, D. Michel, H.C. Semmelhack, G. Völkel, H.J. Gläsel, E. Hartmann, Phys. Rev. B **62** (2000) 2085-2095
[14] (a) R.D. King-Smith, D. Vanderbilt, Phys. Rev. B **47** (1993) 1651; (b) *ibid.* **49** (1994) 5828; (c) D. Vanderbilt, R.D. King-Smith, Phys. Rev. B **48** (1993) 4442
[15] (a) R.E. Cohen, Nature **358** (1992) 136; (b) R.E. Cohen, H. Krakauer, Phys. Rev. B **42** (1990) 6416
[16] (a) W. Zhong, R.D. King-Smith, D. Vanderbilt, Phys. Rev. Lett. **72** (1994) 3618; (b) W. Zhong, D. Vanderbilt, K.M. Rabe, Phys. Rev. Lett. **73** (1994) 1861
[17] U.V. Waghmare, K.M. Rabe, Phys. Rev. B **55** (1997) 6161-6173
[18] C.H. Park, D.J. Chadi, Phys. Rev. B **57** (1998) 13961
[19] S. Pöykkö, D.J. Chadi, Phys. Rev. Lett. **83** (1999) 1231
[20] G. Saghi-Szabo, R.E. Cohen, H. Krakauer, Phys. Rev. Lett. **80** (1998) 4321-4324; *ibid.* Phys. Rev. B **59** (1999) 12771-12776
[21] L. He, D. Vanderbilt, Phys. Rev. B **68** (2003) 134103
[22] S. Pöykkö, D.J. Chadi, Appl. Phys. Lett. **76** (2000) 499-501
[23] E. Cockayne, B.P. Burton, Phys. Rev. B **69** (2004) 144116
[24] C.H. Park, D.J. Chadi, Phys. Rev. Lett. **84** (2000) 4717-4720
[25] A. Abragam, B. Bleaney: *Electron Paramagnetic Resonance of Transition Ions*, Clarendon Press, Oxford (1970)
[26] C. Rudowicz and S. B. Madhu, J. Phys.: Condens. Matter **11**(1999) 273-287
[27] (a) G. Kresse and J. Hafner, Phys. Rev. B **48**, (1993) 13115; (b) G.Kresse and J. Hafner, ibid. **49**, (1994) 14251; (c) G. Kresse and J.Furthmuller, J. Comput. Mater. Sci **6**, (1996) 15 (d) G. Kresse und J. Furthmller, Phys. Rev. B **54**, (1996) 11169
[28] P.E. Blöchl, Phys. Rev. B **50**, (1994) 17953
[29] G. Kresse, and J. Joubert, Phys. Rev. B **59**, (1999) 1758
[30] S.H. Vosko, L. Wilk, M. Nusair, Can. J. Phys. **58** (1980) 1200
[31] M. Methfessel, M. Schilfgaarde and Casali R A. Lecture Notes in Physics **535**, (2000) 114
[32] E. Bott, M. Methfessel, W. Krabs and P. C. Schmidt, J Math Phys. **39**, (1998) 3393
[33] B. Mayer, H. Anton, E. Bott, M. Methfessel, J. Sticht, J.

Harris, P. C. Schmidt, Intermetallics **11**, (2003) 23
[34] O. K. Andersen, Phys. Rev. B **12** (1975) 3060
[35] B. Meyer, D. Vanderbilt, Phys. Rev. B **65** (2002) 104111
[36] J. Kobayashi, R. Ueda, Phys. Rev. **99** (1955) 1900
[37] J. Kobayashi, Y. Uesu, Y. Sakemi, Phys. Rev. B **28** (1983) 3866
[38] S. Ikegami, I. Ueda, T. Miyazawa, J. Phys. Soc. Japan **26** (1969) 1324
[39] A.M. Glazer, S.A. Mabud, Acta Cryst. **B34** (1978) 1065
[40] S.A. Mabud, A.M. Glazer (1979), 12, 49
[41] A. Garcia, D. Vanderbilt, Phys Rev B **54** (1996) 3817
[42] M. Knapp, C. Baehtz, H. Ehrenberg, H. Fuess, J. Synchrotron Rad. **11** (2004) 328-334
[43] A.C. Larson, R.B. von Dreele, LAUR, Los Alamos National Laboratory (1994) 86
[44] P.W. Stephens, J. Appl. Crystallogr. **27** (1999) 462
[45] J.P. Perdew, J.A. Chevary, S.H. Vosko, K.A. Jackson, M.R. Pederson, D.J. Singh, C. Fiolhais, Phys. Rev. B **46** (1992) 6671
[46] J.A. Rodriguez, A. Etxeberriab, L. González and A. Maiti, J. Chem. Phys, **117** (2002) 2699
[47] A.M. Glazer, S.A. Mabud, J. Appl. Cryst. **12** (1979) 49
[48] (a) R.-A. Eichel, H. Kungl, M.J. Hoffmann, J. Appl. Phys. **95** (2004) 8092-8096; (b) R.-A. Eichel, K.-P. Dinse, H. Kungl, M.J. Hoffmann, A. Ozarowski, J. van Tol, L.C. Brunel, Appl. Phys. A **80** (2005) 51-54
[49] R. Merkle, J. Maier, Phys. Chem. Chem. Phys. **5** (2003) 2297-2303
[50] T.J. Yan, V. Gopalan, P.J. Swart, U. Mohideen, Phys. Rev. Lett. **82** (1999) 4106
[51] G.E. Pike, W.L. Warren, D. Dimos, B.A. Tuttle, R. Ramesh, J. Lee, V.G. Keramidas, J.T. Evans, Appl. Phys. Lett. **66** (1995) 484
[52] D.C. Lupascu: *Fatigue in ferroelectric ceramics and related issues*, Springer, Heidelberg (2004)
[53] A.K. Tagantsev, I. Stolichnov, E.L. Colla, N. Setter, J. Appl. Phys. **90** (2001) 1387-1402
[54] D.J. Keeble, B. Nielsen, A. Krishnan, K.G. Lynn, S. Madhukar, R. Ramesh, C.F. Young, Appl. Phys. Lett. **73** (1998) 318
[55] S. Serrano, C. Duque, P. Medina, A. Stashans, SPIE Proceedings **5122** (2002) 287
[56] L. He, D. Vanderbilt, Phys. Rev. B **68** (2003) 134103
[57] R.A. Evarestov, V.P. Smirnov, D.E. Usvyat, Solid State Commun. **127** (2003) 423-426
[58] R.E. Cohen, H. Krakauer, Ferroelectrics **136** (1992) 65
[59] V. Gavrilyachenko, R.I. Spinko, M.A. Martynen, E.G. Fesenko, Sov. Phys. Solid State **12** (1970) 1203
[60] (a) G. Kresse, J. Hafner, Phys. Rev. B **47** (1993) 558; (b) G. Kresse, J. Furthmüller, Phys. Rev. B **54** (1996) 11169
[61] P. Ghosez, J.P. Michenaud, X. Gonze, Phys. Rev. B **58** (1998) 6224
[62] Y. Kuroiwa, S. Aoyagi, A. Sawada, J. Harada, E. Nishibori, M. Takata, M. Sakata, Phys. Rev. Lett. **87** (2001) 217601